The Journal of Chemical Physics

Efficient partitioning technique for computing the dynamics of intramolecular processes: Radiationless transitions in pyrazine

Cite as: J. Chem. Phys. **124**, 184107 (2006); https://doi.org/10.1063/1.2196888
Submitted: 28 February 2006 • Accepted: 23 March 2006 • Published Online: 12 May 2006

P. S. Christopher, Moshe Shapiro and Paul Brumer

View Online Export Citation

ARTICLES YOU MAY BE INTERESTED IN

Quantum control of internal conversion in 24-vibrational-mode pyrazine
The Journal of Chemical Physics **125**, 124310 (2006); https://doi.org/10.1063/1.2346684

Overlapping resonances in the coherent control of radiationless transitions: Internal conversion in pyrazine
The Journal of Chemical Physics **123**, 064313 (2005); https://doi.org/10.1063/1.2000260

Molecular dynamics of pyrazine after excitation to the S_2 electronic state using a realistic 24-mode model Hamiltonian
The Journal of Chemical Physics **110**, 936 (1999); https://doi.org/10.1063/1.478061

Challenge us.
What are your needs for periodic signal detection?
Watch

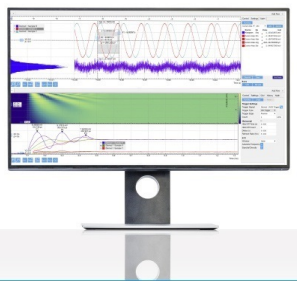

Zurich Instruments

AIP Publishing

© 2006 American Institute of Physics.

Efficient partitioning technique for computing the dynamics of intramolecular processes: Radiationless transitions in pyrazine

P. S. Christopher
Chemical Physics Theory Group, Department of Chemistry, University of Toronto, Toronto, Ontario M5S 3H6, Canada
and Center for Quantum Information and Quantum Control, University of Toronto, Toronto, Ontario M5S 3H6, Canada

Moshe Shapiro
Department of Chemistry, University of British Columbia, Vancouver, British, Columbia V6T 1Z1, Canada
and Department of Chemical Physics, The Weizmann Institute of Science, Rehovot, Israel 76100

Paul Brumer[a)]
Chemical Physics Theory Group, Department of Chemistry, University of Toronto, Toronto, Ontario M5S 3H6, Canada
and Center for Quantum Information and Quantum Control, University of Toronto, Toronto, Ontario M5S 3H6, Canada

(Received 28 February 2006; accepted 23 March 2006; published online 12 May 2006)

An efficient QP partitioning algorithm to compute the eigenvalues, eigenvectors, and the dynamics of large molecular systems of a particular type is presented. Compared to straightforward diagonalization, the algorithm displays favorable scaling ($\propto N_T^2$) as a function of N_T, the size of the Hamiltonian matrix. In addition, the algorithm is trivially parallelizable, necessitating no "cross-talk" between nodes, thus enjoying the full linear speedup of parallelization. Moreover, the method requires very modest storage space, even for extremely large matrices. The method has also been enhanced through the development of a coarse-grained approximation, enabling an increase of the basis set size to unprecedented levels (10^8–10^{10} in the current application). The QP algorithm is applied to the dynamics of electronic internal conversion in a 24 vibrational-mode model of pyrazine. A performance comparison with other dynamical methods is presented, along with results for the decay dynamics of pyrazine and a discussion of resonance line shapes. © *2006 American Institute of Physics*. [DOI: 10.1063/1.2196888]

I. INTRODUCTION

The Löwdin-Feshbach partitioning technique[1–7] has a long and impressive history in chemical physics. It allows one to focus on a specific system while taking into account its coupling to the surroundings through effective matrix elements. In the past the partitioning technique was mainly used as a starting point for further approximations—through some perturbation strategy and/or through an estimation of system-environment effects. In contrast, this paper presents a numerical method based on the partitioning technique, which we term the QP algorithm, which allows the accurate computation of bound state Hamiltonian eigenvalues and eigenvectors for large molecular systems. Given the eigenvalues and eigenvectors, the computation of system dynamics for large numbers of different initial states becomes a straightforward task.

For the class of problems considered, the algorithm described below has a number of computationally impressive characteristics. Specifically, it has excellent scaling properties as compared to conventional diagonalization techniques, it admits a quasicontinuum extension that allows for extremely large basis expansions, it is trivially parallelizable, and it requires very modest storage space, even for extremely large matrices. As a result, the QP algorithm provides a useful tool to tackle the full quantum dynamics of large molecular systems. As an example, we apply the method to S_2 to S_1 internal conversion (IC) of full 24 vibrational-mode pyrazine, using the potential of Raab *et al.*[8]

The QP algorithm, by providing system eigenstates and eigenvalues, allows for studies of wave packet dynamics of a wide range of initial preparations with little additional computational overhead. Moreover, by subdividing the system into a relevant component ("the Q space") and a less relevant component ("the P space") the method allows for a transparent physical interpretation via the direct analysis of the effect of the P space on the Q space, most often seen as resonance broadening of the Q-space states.

In applying this method we have focused on pyrazine, whose photophysics has been a subject of long standing interest. Of particular interest is the ultrafast dynamics following the optical excitation of pyrazine from the ground state S_0 to the second excited singlet state S_2. The process of IC from S_2 to the first excited singlet state S_1 at time scales estimated experimentally to be 20 fs (Ref. 9) then follows. A great deal of theoretical work has gone into understanding these experimental findings.[8,10–12]

Our interest in pyrazine also stems from past studies in

[a)]Electronic mail: pbrumer@tikva.chem.utoronto.ca

 © 2006 American Institute of Physics

which we computationally demonstrated coherent control[13] of the IC process in a four-mode model.[14] In particular, we demonstrated that the extent of phase control over the flow out of the S_2 manifold depends on the participation of *overlapping resonances*. At that time our studies were limited to the four-mode model because of the enormity of the density of states in the S_1 manifold ($>10^6$ cm^{-1}), prohibiting the straightforward diagonalization of the full problem by conventional techniques. In contrast, the QP algorithm developed here allows for the treatment of the $\sim 10^{10}$ states associated with the full 24-mode problem. Our studies of coherent control in the 24-mode problem will be described elsewhere.[15]

This paper is organized as follows. Section II describes the theory and methodology of the QP algorithm. Specifically, Sec. II A summarizes the equations of the Löwdin-Feshbach partitioning technique, Sec. II B describes the QP algorithm and emphasizes the requirement that the P space be readily diagonalizable, Sec. II C outlines the coarse-grained approximation, and Sec. II D describes the pyrazine model used in this paper. Section III contains the results of our investigations on pyrazine. In particular, we present the autocorrelation function and diabatic populations as a function of time and compare these results with results using wave packet propagation methods. The performance of the QP algorithm is shown to be far superior to other methods. The resonance structure of pyrazine is discussed at the end of this section. Finally, Sec. IV concludes the paper and includes suggestions for future work.

II. THEORY, ALGORITHM, AND COMPUTATIONAL DETAILS

In order to simplify the description of the QP algorithm, we present it in the framework of the IC dynamics of pyrazine. Generalization to other molecules, and other physical processes, should be obvious.

Pyrazine $C_4N_2H_6$ has a benzenelike structure, with the ring composed of four carbons and two nitrogens, the latter being opposite to one another on the ring. The molecule has 24 vibrational normal modes, each classified into one of eight different irreducible representations (irrep) of the D_{2h} point group. Excitation from S_0 preferentially populates S_2 vibrational states, rather than S_1 states, because the electronic transition dipole moment of the former is much larger than the latter. As a consequence, one can safely approximate the state of the system after excitation as a superposition of vibrational states belonging to the S_2 manifold. Rotational levels are neglected in this discussion. As mentioned above, due to the conical intersection of the S_1 and S_2 surfaces, population in vibrational states prepared on S_2 undergo a (10–40 fs) rapid transition to the S_1 states.

A. The Löwdin-Feshbach partitioning

Let H be the full Hamiltonian of the system, and $\{|\gamma\rangle\}$ and $\{E_\gamma\}$ be its eigenstates and eigenenergies,

$$H|\gamma\rangle = E_\gamma|\gamma\rangle. \tag{1}$$

The full Hilbert space of the system can be divided into two subspaces using projection operators Q and P, with $P+Q=1$. In the pyrazine case the Q space contains vibrational states of the S_2 electronic manifold, and the P space comprises the vibrational states of the S_1 electronic manifold. The states $\{|\kappa\rangle\}$ denote the basis for the Q space with projector Q given by

$$Q = \sum_\kappa |\kappa\rangle\langle\kappa|. \tag{2}$$

Similarly the $\{|\beta\rangle\}$ states span the P space with projector P given by

$$P = \sum_\beta |\beta\rangle\langle\beta|. \tag{3}$$

Consider the nuclear Hamiltonian

$$H = H_0 + V_{\mathrm{IC}}, \tag{4}$$

where H_0 is the sum of Hamiltonians on the two electronic surfaces and V_{IC} couples basis states between the two surfaces. With this definition it is obvious that $QHQ=QH_0Q$, $PHP=PH_0P$, and $QHP=QV_{\mathrm{IC}}P$ which are described, respectively, as the Hamiltonian on S_2, the Hamiltonian on S_1, and the IC coupling. The bases $\{|\kappa\rangle\}$ and $\{|\beta\rangle\}$ are chosen to diagonalize the noninteracting parts of the Hamiltonian:

$$QHQ|\kappa\rangle = \epsilon_\kappa|\kappa\rangle, \tag{5}$$

$$PHP|\beta\rangle = \epsilon_\beta|\beta\rangle. \tag{6}$$

Below, we denote the dimensions of the Q space and P space as N_Q and N_P, respectively.

As summarized in Appendix A, application of the Q and P projection operators to Eq. (1) yields an eigenvalue equation for the states $Q|\gamma\rangle$, i.e., the projection of $|\gamma\rangle$ onto the Q space. Specifically,

$$(E_\gamma - \tilde{H}(E_\gamma))Q|\gamma\rangle = 0, \tag{7}$$

where, for the bound state case,

$$\tilde{H}_{\kappa\kappa'}(E_\gamma) = \epsilon_\kappa\delta_{\kappa\kappa'} + \sum_\beta \frac{V_{\kappa\beta}V^*_{\kappa'\beta}}{E_\gamma - \epsilon_\beta}, \tag{8}$$

$$V_{\kappa\beta} \equiv \langle\kappa|V_{\mathrm{IC}}|\beta\rangle. \tag{9}$$

From a computational standpoint, the main advantage of Eq. (7) over Eq. (1) is that the eigenvalue problem in Eq. (7) is of dimension N_Q, whereas the full eigenvalue equation in Eq. (1) is of dimension of $N_T=N_P+N_Q$. Since the best general diagonalization methods scale as the cube of the matrix dimension: this scaling being estimated[16] as $25N^3$, this approach provides a significant advantage.[18] Hence, if $N_Q \ll N_P$, as in the problems discuss below, Eq. (7) shows significant savings over straightforward diagonalization.

The price one pays in dealing with Eq. (7) is the need to diagonalize $\tilde{H}$ which is a function of the (as yet) unknown E_γ eigenvalues. Indeed, this is one of the reasons why the Feshbach formalism has been mainly applied to continuum

problems, where every energy is an eigenenergy. An algorithm for bound state problems based on Eq. (7) must be able to solve these implicit eigenvalue equations efficiently.

B. The QP algorithm

One could imagine solving Eq. (7) by using self-consistent iteration. That is, one could (a) use a trial energy $E_\gamma^{(i)}$, (b) diagonalize $\tilde{H}(E_\gamma^{(i)})$, (c) choose one of its eigenvalues to be $E_\gamma^{(i+1)}$, and (d) iterate this procedure until the system converged onto a stationary point. We have already successfully applied this approach to intramolecular vibrational redistribution in carbonyl sulfide.[19] Empirically, however, this procedure was found to be fairly unstable for larger problems. It is difficult to obtain most of the eigenvalues in this manner, and in addition, the number of iterations per eigenvalue seemed to increase with the dimension of the P space.

Consider, instead, performing the above search on a full vector of eigenvalues. In such a method one first selects an energy ϵ and then diagonalizes the entire $\tilde{H}(\epsilon)$ matrix to obtain a vector of eigenenergies, $\underline{\epsilon'}$. One then computes the difference between the input energy and the output energies. Symbolically this is represented as

$$\epsilon \Rightarrow \tilde{H}(\epsilon) \Rightarrow \underline{\epsilon'} \Rightarrow \underline{\Delta}(\epsilon), \tag{10}$$

where

$$\underline{\Delta}(\epsilon) = \epsilon \underline{1} - \underline{\epsilon'}. \tag{11}$$

Here, any ϵ that gives a zero in one of the $\underline{\Delta}$ components corresponds to an eigenvalue of the full Hamiltonian. Provided that $\underline{\Delta}$ is reasonably well behaved as a function of energy, finding all the ϵ for which $\underline{\Delta}_k(\epsilon)=0$ amounts to finding all the eigenvalues of the full Hamiltonian of Eq. (1). Further, it is relatively easy to search for solutions of $\underline{\Delta}_k(\epsilon)=0$: we lays down a grid of energies ϵ_i, search for pairs of grid points that bracket a solution, and use bisection to refine the solution.

One problem that arises with this procedure is that the order of energies in $\underline{\epsilon'}$ can change from one energy grid point to the next upon iteration. Since the algorithm compares the values of $\underline{\Delta}$ element by element, if the order of components in $\underline{\epsilon'}$ changes between grid points, this could result in missing some eigenvalues.[20] In order to rectify this situation, we use the eigenvectors of $\tilde{H}(\epsilon_{i-1})$ to order the energies in the vector $\underline{\epsilon}_i^f$. This procedure is symbolized by the expression

$$\epsilon_i, \underline{\underline{\chi}}_{i-1} \Rightarrow \tilde{H}(\epsilon_i) \Rightarrow \underline{\epsilon}_i', \underline{\underline{\chi}}_i \Rightarrow \underline{\Delta}(\epsilon), \tag{12}$$

where $\underline{\underline{\chi}}_i$ is the eigenvector matrix of $\tilde{H}(\epsilon_i)$. We order $\underline{\epsilon}_i'$ by comparing the scalar products of the various i and $(i-1)$ eigenvectors. Specifically, the eigenvalue that is put into the kth position of $\underline{\epsilon}_i'$ is that eigenvalue whose eigenvector, $\underline{\chi}_{ij}$, has maximal overlap with the kth eigenvector of the last iteration, $\underline{\chi}_{(i-1)k}$.

Once the solver converges on a $\underline{\Delta}_k(\epsilon)=0$ solution both the eigenenergy and a vector proportional to $Q|\gamma\rangle$ are obtained. The proportionality factor is then obtained as described in Appendix C. Further, given $Q|\gamma\rangle$, one can efficiently compute the entire vector $|\gamma\rangle$ through the use of Eq. (A4) of Appendix A. Below, however, we focus solely on $Q|\gamma\rangle$.

Since there is no guarantee that all the solutions of $\underline{\Delta}_k(\epsilon)=0$ will be found with a given grid of energy points, there is no guarantee that all the eigenstates of the system will be found. However, it is an empirical fact that the larger the Q-space overlap of a particular eigenstate $|\gamma\rangle$, the easier it is to find that particular eigenstate using the QP algorithm. Thus, fortunately, the most important eigenstates necessary to describe the Q-space dynamics are relatively easy to find. In practice, in order to assess the quality of the eigenvector coverage, we employ the metric

$$\sum_{\gamma\in F} \langle\kappa|\gamma\rangle\langle\gamma|\kappa'\rangle = \sum_{\gamma\in F} \langle\kappa|Q|\gamma\rangle\langle\gamma|Q|\kappa'\rangle, \tag{13}$$

where F is the set of labels of eigenstates that have been found by the algorithm. As F approaches a perfect description of the Q-space dynamics, the expression of Eq. (13) approaches $\delta_{\kappa\kappa'}$.

Although we saw no degeneracy in the numerical results presented below, for completeness we comment on how degeneracy manifests itself in the QP algorithm. If the full Hamiltonian H has a degeneracy then this would appear as a degeneracy in the effective Hamiltonian $\tilde{H}$. For example, if the full Hamiltonian has a double degeneracy at E_d, $\tilde{H}(E_d)$ would have a doubly degenerate eigenvalue. Given this behavior, what happens if the full Hamiltonian has a degeneracy greater than N_Q? Clearly the formalism is exact for all Hamiltonians, yet it is perfectly possible to envisage Hamiltonians with degeneracies larger than N_Q, whereas $\tilde{H}(E)$ is of dimension N_Q. The resolution to this paradox proven in Appendix B is that given a set of $M>N_Q$ degenerate eigenstates, one can always reconstruct this set so that at most N_Q of them have a nonzero Q-space overlap. In this way the degeneracy of $\tilde{H}(E)$ cannot exceed N_Q.

The performance of the QP algorithm must be measured against the performance of straightforward diagonalization techniques which scale[16] as $25N_T^3$, with $N_T=N_Q+N_P$. In order to estimate the performance of the QP algorithm, one conceives of using KN_T grid points,[21] where K is a positive constant. One then searches these grid points for $\underline{\Delta}$ zeros.

The total numerical effort required by the QP algorithm can thus be computed as follows.

(1) The numerical effort of computing each $\underline{\Delta}$ can be written as $C_1N_Q^3+C_2N_Q^2N_P$ (with C_1 and C_2 constants typical to the problem). This number is made up of the effort of building $\tilde{H}$, which scales as $N_Q^2N_P$ ($\tilde{H}$ has N_Q^2 matrix elements, each being a sum of N_P terms), and the effort in diagonalizing $\tilde{H}$, which scales as N_Q^3.
(2) The effort involved in computing $KN_T\underline{\Delta}$ vectors is $KN_T(C_1N_Q^3+C_2N_Q^2N_P)$.
(3) The effort in refining N_T solutions. If M is the average number of $\underline{\Delta}$ evaluations required to refine a solution, we obtain that the total cost of the refinement phase is $MN_T(C_1N_Q^3+C_2N_Q^2N_P)$.
(4) The sum total of items (2) and (3) (noting that K and M

are independent of N_T) is therefore $N_T(K+M)(C_1N_Q^3 + C_2N_Q^2N_P)$.

Thus for $N_P \gg N_Q$, the QP algorithm scales like $N_P^2 \approx N_T^2$, giving linear speedup over straightforward diagonalization. We see that the performance[22] of the QP algorithm is superior to conventional methods only if N_Q is small compared to N_P, i.e., when a smaller subspace is coupled to a far larger subspace. In addition to possessing a good scaling behavior, the QP algorithm is highly parallelizable, requiring very modest storage space. These parameters are especially favorable to the clusters of personal computer nodes available nowadays to most researchers.

In assessing the algorithm performance, we have not included the time associated with diagonalizing the P space. Here it is assumed that the P space is diagonal or can be diagonalized, as in the pyrazine case below, in times short compared to the other operations.

In the parallelized version of the algorithm each node receives a copy of the Hamiltonian and a list of energy grid points to search. Each node can then work in isolation until it has completed its grid point list. Then, at the end of the calculation, all the resultant eigenvectors/eigenvalues are harvested from the nodes. This itinerary requires very little internode communication, allowing for highly efficient parallelization.

The success of the QP algorithm depends critically on our ability to efficiently compute the $(E_\gamma - PHP)^{-1}$ part of $\tilde{H}$ [see Eq. (A7)]. This is trivially the case if the PHP matrix can be diagonalized analytically (e.g., the P space is composed of harmonic modes). Even if PHP cannot be diagonalized analytically, the method is very efficient if one can diagonalize individual pieces of PHP, as illustrated below for pyrazine. Alternatively, if this is not the case, but the various P-space couplings are relatively weak compared to level spacing, one can use perturbation theory to obtain a new basis which approximately diagonalizes PHP. In first order perturbation theory, for example, the coupling Hamiltonian elements are given by

$$\langle \kappa | V_{\mathrm{IC}} | \beta^{(1)} \rangle = \langle \kappa | V_{\mathrm{IC}} | \beta \rangle + \sum_{\beta' \in W_\beta} \frac{\langle \kappa | V_{\mathrm{IC}} | \beta' \rangle \langle \beta' | H_0 | \beta \rangle}{\epsilon_\beta - \epsilon_{\beta'}}, \tag{14}$$

where $|\beta^{(1)}\rangle$ is the first order correction to $|\beta\rangle$, W_β is a window of nearby states[23] which does not include β, and where we assume that there is no degeneracy in the Hamiltonian (the degenerate formulas being obvious extensions).

Given that the P space is diagonal, and thus contains many zeros, one might assume that there are direct eigenstate methods that scale better than N_T^3, and thus that there is a direct route to diagonalizing the full Hamiltonian. This is, however, not the case. There are, of course, methods that allow one to diagonalize large matrices efficiently for certain highly zeroed matrix symmetries (tridiagonal, banded, etc.). However, to the authors' knowledge, there is no way to efficiently diagonalize, directly, matrices of the symmetry that is presented in this paper. Furthermore, as is presented in the next section, the QP algorithm allows a coarse-grained approximation that allows one to consider matrices with dimension greater than 10^{10}, i.e., matrices so large that there are no known methods to compute the dynamically important eigenstates of the system.

C. Coarse graining

Although the QP algorithm allows one to handle a much higher number of states than in straightforward diagonalizations, the actual density of states in the P space can still be too large even for this method. Such is the case for the 24-mode pyrazine treated below. Fortunately, because the density of states is so high, we are able to invoke a quasicontinuum approximation by which we effectively coarse grain the Hamiltonian. The idea is to divide up the energy axis into small bins A_m, centered at energy ε_m, and represent all the coupling Hamiltonian matrix elements in each bin by a single term. This process can radically reduce N_P with, for time scales of interest to us, negligible effect on the results.

The coarse graining is performed by approximating Eq. (8) as

$$\begin{aligned}\tilde{H}_{\kappa\kappa'}(E_\gamma) &= \epsilon_\kappa \delta_{\kappa\kappa'} + \sum_\beta \frac{V_{\kappa\beta} V^*_{\kappa'\beta}}{E_\gamma - \epsilon_\beta} \\ &\approx \epsilon_\kappa \delta_{\kappa\kappa'} + \sum_m \frac{1}{E_\gamma - \varepsilon_m} \sum_{\beta \in A_m} V_{\kappa\beta} V^*_{\kappa'\beta} \\ &= \epsilon_\kappa \delta_{\kappa\kappa'} + \sum_m \frac{1}{E_\gamma - \varepsilon_m} \Gamma_{m,\kappa,\kappa'},\end{aligned} \tag{15}$$

where $\Gamma_{m,\kappa,\kappa'}$, implicitly defined in Eq. (15), is the *coarse-grained* coupling matrix. The approximation invoked in Eq. (15) is good as long as the width of the bins is small; it becomes exact as the width of the bins approaches zero.

In order to describe the system dynamics, a connection between the solutions of Eq. (15) and the set of exact eigenstates $\{|\gamma\rangle\}$ must be established. To do so, we define the coarse-grained projectors $|\alpha\rangle\langle\alpha|$ as

$$|\alpha\rangle\langle\alpha| = \frac{1}{\varrho_\alpha \Delta_\alpha} \sum_{\gamma \in A_\alpha} |\gamma\rangle\langle\gamma|, \tag{16}$$

where ϱ_α is the density of states of bin A_α, Δ_α is the width of bin A_α, and $|\gamma\rangle$ are the true eigenstates of the system. The definition of Eq. (16) has the important property that

$$\sum_\alpha \varrho_\alpha \Delta_\alpha |\alpha\rangle\langle\alpha| = \hat{I}, \tag{17}$$

where $\hat{I}$ is the identity operator.[24] The *ansatz* that we invoke in order to connect the coarse-grained states with the QP algorithm is that the eigenstates that are obtained from the (coarse-grained Hamiltonian) QP algorithm are equal to $\sqrt{\varrho_\alpha \Delta_\alpha}|\alpha\rangle$. Our confidence in this protocol comes from the many model systems that we have studied for which it has proven to be correct.

The dynamics of the system are obtained from the $\langle \kappa' | U(t) | \kappa \rangle$ evolution operator matrix elements, where in (a.u.) $U(t) = e^{-iHt}$. The analogous matrix elements within the coarse-grained dynamics are defined as

$$\langle\kappa'|U(t)|\kappa\rangle = \sum_{\alpha}\sum_{\gamma\in A_\alpha}\langle\kappa'|\gamma\rangle\langle\gamma|\kappa\rangle e^{-iE_\gamma t}$$
$$= \sum_{\alpha}\varrho_\alpha\Delta_\alpha\langle\kappa'|U(t)|\alpha\rangle\langle\alpha|\kappa\rangle$$
$$\approx \sum_{\alpha}B_\alpha(\kappa',\kappa)\varrho_\alpha\sum_{\gamma\in A_\alpha}\frac{e^{-iE_\gamma t}}{\varrho_\alpha}. \quad (18)$$

The above formula amounts to replacing $\langle\kappa'|\gamma\rangle\langle\gamma|\kappa\rangle$ by $B_\alpha(\kappa',\kappa)$, its average value in bin A_α, given by

$$B_\alpha(\kappa',\kappa)\equiv\langle\kappa'|\alpha\rangle\langle\alpha|\kappa\rangle = \frac{1}{\varrho_\alpha\Delta_\alpha}\sum_{\gamma\in A_\alpha}\langle\kappa'|\gamma\rangle\langle\gamma|\kappa\rangle. \quad (19)$$

The final sum of Eq. (18) can be approximated if one assumes that there are many eigenvalues distributed evenly over the bin. In this case one writes

$$\frac{1}{\Delta_\alpha}\sum_{\gamma\in A_\alpha}\frac{e^{-iE_\gamma t}}{\varrho_\alpha}\approx\frac{1}{\Delta_\alpha}\int_{\varepsilon_\alpha-\Delta_\alpha/2}^{\varepsilon_\alpha+\Delta_\alpha/2}dEe^{-iEt} = \frac{e^{-i\varepsilon_\alpha t}\sin(\Delta_\alpha t/2)}{\Delta_\alpha t/2}$$
$$\equiv\tau_\alpha(t), \quad (20)$$

giving, finally,

$$\langle\kappa'|U(t)|\kappa\rangle = \sum_{\alpha}B_\alpha(\kappa',\kappa)\varrho_\alpha\Delta_\alpha\tau_\alpha(t). \quad (21)$$

Note that with the assumption above there is no need to know $\varrho_\alpha\Delta_\alpha$. Rather, the QP algorithm, in fact, delivers $\sqrt{\varrho_\alpha\Delta_\alpha}|\alpha\rangle$. In fact, we have maintained the $\varrho_\alpha\Delta_\alpha$ product form so that the trace of $|\alpha\rangle\langle\alpha|$ is manifestly equal to 1.

It is important to realize that the approximations made in deriving Eq. (21) improve as $\Delta_\alpha t$ decreases. For all the calculations presented in this paper, errors introduced by these approximations can be shown to be negligible since the time scale we look at in this paper is such that $\Delta_\alpha t$ is small. This fact can be appreciated by considering two eigenstates, one on each side of bin A_α. In this case, the contribution to the transition amplitude of the first line of Eq. (18) is

$$\langle\kappa'|U(t)|\kappa\rangle = \langle\kappa'|1\rangle\langle1|\kappa\rangle\exp[-i(\varepsilon_\alpha+\Delta_\alpha/2)t]$$
$$+\langle\kappa'|2\rangle\langle2|\kappa\rangle\exp[-i(\varepsilon_\alpha-\Delta_\alpha/2)t]$$
$$=\exp(-i\varepsilon_\alpha t)[\langle\kappa'|1\rangle\langle1|\kappa\rangle\exp(-i\Delta_\alpha t/2)$$
$$+\langle\kappa'|2\rangle\langle2|\kappa\rangle\exp(i\Delta_\alpha t/2)]. \quad (22)$$

We thus have that as long as $\Delta_\alpha t\ll1$,

$$\langle\kappa'|U(t)|\kappa\rangle\approx\exp(-i\varepsilon_\alpha t)[\langle\kappa'|1\rangle\langle1|\kappa\rangle+\langle\kappa'|2\rangle\langle2|\kappa\rangle], \quad (23)$$

which is analogous to a single term of Eq. (21) because if $\Delta_\alpha t$ is small then $\tau_\alpha(t)\approx e^{-i\epsilon_\alpha t}$, and because in this case $\Delta_\alpha\varrho_\alpha=2$. The above condition holds for the calculations presented below where $\Delta_\alpha\approx10^{-4}$ eV and $t\leqslant2\times10^2$ eV^{-1} (150 fs). Thus for our calculations the phase differences between neighboring points in a bin are negligible.

D. The pyrazine model

We now consider IC in the 24-mode model of pyrazine of Raab *et al.*[8] The model describes pyrazine as composed of normal modes, coupled by terms represented as polynomials whose coefficients are made to fit the *ab initio* calculation. The Hamiltonian for the system is given by

$$H=\sum_i\begin{pmatrix}1&0\\0&1\end{pmatrix}\frac{\omega_i}{2}\left(\frac{\partial^2}{\partial Q_i^2}+Q_i^2\right)+\begin{pmatrix}-\Delta&0\\0&\Delta\end{pmatrix}$$
$$+\sum_{i\in G_1}\begin{pmatrix}a_i&0\\0&b_i\end{pmatrix}Q_i+\sum_{i,j\in G_2}\begin{pmatrix}a_{ij}&0\\0&b_{ij}\end{pmatrix}Q_iQ_j$$
$$+\begin{pmatrix}0&\lambda_{10a}\\\lambda_{10a}&0\end{pmatrix}Q_{10a}+\sum_{i,j\in G_4}\begin{pmatrix}0&c_{ij}\\c_{ij}&0\end{pmatrix}Q_iQ_j, \quad (24)$$

where ω_i are the normal mode frequencies of S_0, Q_i are the dimensionless normal coordinates on S_0, 2Δ is the energy difference between the S_2 and S_1 surfaces, a_i, b_i, a_{ij}, and b_{ij} are the coupling constants within each electronic manifold, and λ_{10a} and c_{ij} are the coupling terms between different electronic states. We denote by G_1 the set of normal modes that have A_g symmetry, by G_2, the set of pairs of modes that have the same symmetry, and by G_4 all pairs of modes whose product is of B_{1G} symmetry. It is important to note that the most significant contributions to the system dynamics are the harmonic oscillator terms and the linear terms a_i, b_i, and λ_{10a}; the other terms, a_{ij}, b_{ij}, and c_{ij} are less relevant. Nonetheless, all the terms in the Hamiltonian of Raab *et al.* are included in the computations below. (The linear coupling terms within each electronic state are necessary, as shown by our lack of success in modeling pyrazine dynamics using the model of Borrelli and Peluso[25] which lacks these terms.) The structure of the on-surface coupling allows for a relatively easy diagonalization of *PHP* because the coupling terms within each electronic states only couple modes of the same irreducible representation.

The *PHP* part of the Hamiltonian of Eq. (24) can be written as

$$PHP=\sum_{i=1}^{8}PH_iP, \quad (25)$$

where i ranges over the eight irreducible representations (irreps). One can diagonalize each PH_iP as

$$PH_iP|\phi_k^{(i)}\rangle = e_k^{(i)}|\phi_k^{(i)}\rangle. \quad (26)$$

With the $|\phi^{(i)}\rangle$ in hand, we form the total eigenstates $|\eta\rangle$ as

$$|\eta_s\rangle = |\phi_{k_1}^{(1)}\rangle|\phi_{k_2}^{(2)}\rangle\ldots|\phi_{k_8}^{(8)}\rangle = \prod_{i=1}^{8}|\phi_{k(s)}^{(i)}\rangle, \quad (27)$$

with

$$PHP|\eta_s\rangle = E_s|\eta_s\rangle \quad (28)$$

and $E_s=\Sigma_i e_{k(s)}^{(i)}$. Here $k(s)$ denotes the collection of eight k values $(k_1,k_2,\ldots,k_8)$ labeling the contribution to $|\eta_s\rangle$ of particular eigenstates of PH_iP. Analogous results can be obtained in diagonalizing *QHQ*. Constructing a basis that spans all 24 modes is then a simple matter of taking a product basis

of the individual irrep eigenstates, a process done for both S_1 and S_2. This procedure was facilitated by the fact that handling a particular irrep required diagonalizing a matrix of only modest size (always less than 7000 elements).

With this in mind, we can describe the full procedure for constructing the Hamiltonian. First, a harmonic oscillator basis is selected by taking all basis states whose energy was less than some cutoff value, here taken to be 1.9 eV, where the threshold of S_1 is at $E=0.0$ eV and that of S_2 is at $E=0.846$ eV. Next the Hamiltonian within each electronic state for each irrep is constructed and diagonalized. This diagonalizes both *QHQ* and *PHP*. Given $|\eta^{(1)}\rangle$ and $|\eta^{(2)}\rangle$, the eigenstates which diagonalize the decoupled S_1 and S_2 manifolds, we compute *QHP* for an η basis defined as

$$|\eta_s^{(1)}\rangle = \sum_\beta C_{s\beta}^{(1)}|\beta\rangle, \tag{29}$$

$$|\eta_s^{(2)}\rangle = \sum_\kappa C_{s\kappa}^{(2)}|\kappa\rangle, \tag{30}$$

$$[QHP]_{mn} = \langle \eta_m^{(2)}|H|\eta_n^{(1)}\rangle = \sum_{\kappa\beta} (C_{m\beta}^{(2)})^* C_{n\kappa}^{(1)} V_{\kappa\beta}, \tag{31}$$

where the C's are the expansion coefficients of the $|\eta\rangle$ states in the bare states $|\kappa\rangle$ or $|\beta\rangle$. This process results in diagonal *QHQ* and *PHP* matrices and off-diagonal block *QHP*—all expressed in the $|\eta\rangle$ basis.

For purposes of comparing with previous results we chose the Q space to be composed of the 176 vibrational states of S_2 that have the largest Franck-Condon overlap with $|S_0;0\rangle$, where $|S_0;0\rangle$ is the ground vibrational state of S_0. We define the autocorrelation function as

$$J(t) \equiv |\langle\psi(0)|U(t)|\psi(0)\rangle| \tag{32}$$

for some initial state $|\psi(0)\rangle$. The 176 basis states chosen yielded a $J(t)$ for $|\psi(0)\rangle=|S_0;0\rangle$, in good agreement to that obtained in Ref. 26. In comparison, when we used a basis of 28 basis states, the behavior of J after about 15 fs (the initial decay) was noticeably different from that of Ref. 26. This result highlights an important issue in selecting a Q-space basis for a decay problem: the resonances in the Q-space basis interfere with one another. Hence, the resonance line shape of a particular Q-space state can change depending on which other resonances are included in the calculation.

III. RESULTS

We first studied the QP algorithm for a variety of model systems, choosing assorted values of N_Q and N_P, bare energies $\{\epsilon_\beta\}$, and coupling matrix elements $V_{\kappa\beta}$. The energies $\{\epsilon_\beta\}$ were either chosen to be evenly spaced or randomly distributed, and $V_{\kappa\beta}$ was chosen to have constant, Gaussian, sinusoidal, or random functional forms, or products of these. In all these cases the QP algorithm successfully generated the eigenstates of the system, while displaying the scaling behavior discussed above. Further, for each of the model systems, we tested the coarse-grained approximation by comparing it to an exact calculation with some N_P for which $n_{\text{bins}} \ll N_P$ was satisfied. The agreement of the coarse-grained and exact results was very good for all the calculations we have performed. In particular, similar resonance line shapes and similar dynamical evolution, which got better with increasing n_{bins}/N_P, were obtained. These results support the arguments of Sec. II C.

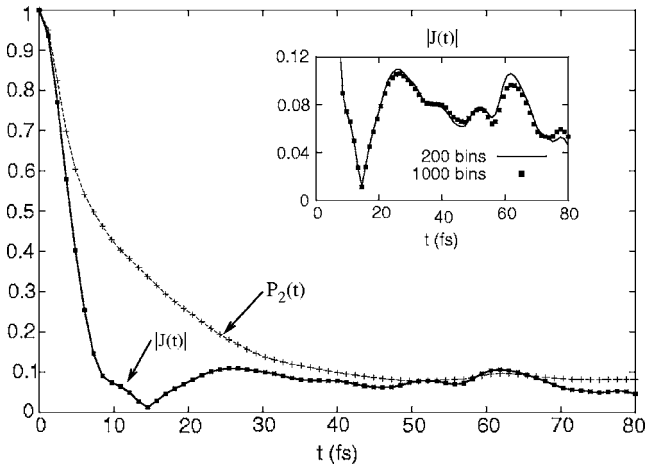

FIG. 1. (Main) $J(t)$ (dark line) and $P_2(t)$ (light line) for the $|S_0;0\rangle$ initial state. (Inset) Comparison of $J(t)$ for 200 and 1000 bins.

A. Numerical performance tests

Below we present the autocorrelation function $J(t)$ as well as the diabatic population $P_2(t)$,

$$P_2(t) = \langle\psi(t)|Q|\psi(t)\rangle, \tag{33}$$

i.e., the probability of finding the system in any state in S_2 at time t.

Figure 1 displays our computed $J(t)$, [Eq. (32)], and $P_2(t)$, [Eq. (33)], as functions of time for $|\psi(0)\rangle=|S_0;0\rangle$. Our $J(t)$ plot is in excellent agreement with the equivalent multiconfiguration time dependent Hartree (MCTDH) results in Fig. 6 of Ref. 26, with the small differences arising from our use of only 176 $|\eta\rangle$ basis states in the Q space, yielding a $\Sigma_\eta|\langle\eta|S_0;0\rangle|^2$ of about 0.8. Achieving $\Sigma_\eta|\langle\eta|S_0;0\rangle|^2=1$ would require an enormous number of Q states, as the $|S_0;0\rangle$ state expansion converges very slowly after the first 170 states. Such convergence studies were not undertaken since, in any event, a $|\psi(0)\rangle=|S_0;0\rangle$ initial condition is unphysical insofar as it would arise only from a $\delta(t)$ laser pulse.

Unless otherwise specified, in all the calculations reported below the Hamiltonian was coarse grained over a range of ~2 eV into 200 bins, giving rise to eigenvalues that were typically spaced by $\approx 10^{-4}$ eV. A comparison of the results for 200 vs 1000 bins is shown in Fig. 1, supporting the reliability of the 200 bin results.

We have compared the QP algorithm with two other methods used in the past to solve the pyrazine dynamics with the Hamiltonian of Raab *et al.*: the semiclassical method of Thoss *et al.*,[26] and the quantum MCTDH method of Raab *et al.*[8] When distributed over forty 1.8 GHz AMD Opteron processors, in a vanilla Beowulf configuration, the parallelized QP calculation of the eigenstates used to generate Fig. 1 takes only 40 min. This is equivalent to 27 CPU hours were the method to be run with a single processor. (We note that the added serial time for diagonalizing the P-space Hamil-

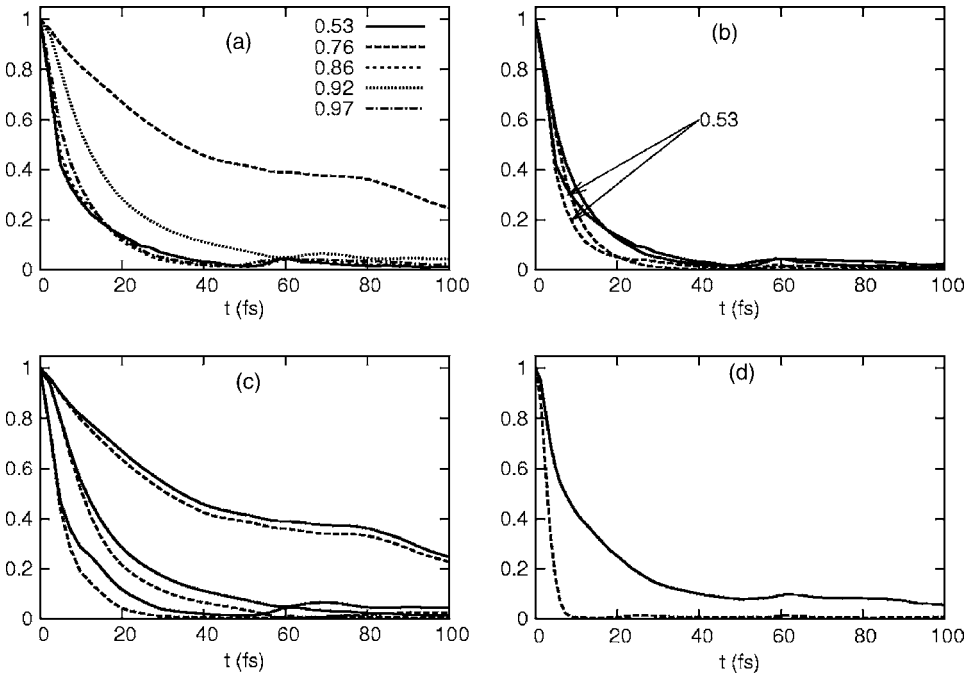

FIG. 2. (a) $P_2(t)$ for several S_2 states. The states are labeled according to their energy. (b) $P_2(t)$ (solid line) and $J(t)^2$ (dashed line) for the states at 0.53 and 0.97 eV. These are the two states whose resonances are pictured in Fig. 3. Arrows point at $J(t)$ and $P_2(t)$ of the 0.53 eV state. (c) $P_2(t)$ (solid line) and $J(t)^2$ (dashed line) for states at 0.76, 0.86, and 0.92 eV. The 0.76 eV state is pictured in Fig. 6. (d) $P_2(t)$ and $J(t)^2$ for the $|S_0;0\rangle$ state in Fig. 1.

tonian and coarse graining the Hamiltonian is approximately 2.3 CPU hours.) For comparison, the MCTDH calculations took 485 CPU hours on a Cray T90 shared-memory machine.[27] We conservatively estimate that modern hardware would give a factor of 2–3 performance increase of the MCTDH calculations. This still results in a six- to ninefold efficiency improvement of the QP method relative to that of MCTDH. The semiclassical method of Thoss *et al.*, which is apparently more computationally costly than the MCTDH method, is outperformed by the QP algorithm by an even larger margin.

Even more important than the serial performance is the parallel performance of the QP algorithm. From the operational perspective, the wall time, not the serial time, is the relevant quantity. We do not expect MCTDH to benefit nearly as significantly from parallelization as does the QP algorithm. This is because the MCTDH method, in which one solves a set of first order nonlinear coupled differential equations, requires a large degree of internode communication, thereby destroying the linear speedup with the number of nodes that is enjoyed by the QP algorithm.

An additional important point is that the QP algorithm provides system eigenvalues and eigenstates, which, once determined, can be used to obtain assorted $|\psi(t)\rangle$ at very little additional cost. That is, once the eigenvalues and eigenstates are known, calculations of $P_2(t)$ of additional initial $|\kappa\rangle \in S_2$ states take less than 4 min to complete, and $J(t)$ computations are on the order of seconds.

Figure 2(a) displays $P_2(t)$ for several initial states, labeled by their energy on the decoupled S_2 manifold. Panel (A) shows the wide diversity of $P_2(t)$ falloff for different initial states. In comparing $P_2(t)$ to $J(t)^2$ we note that the decay of $J(t)^2$ with time can be attributed entirely to Q-P IC coupling. This means, as discussed in our earlier paper,[14] that the difference $[P_2(t)-J(t)^2]$ indicates the amount of IC recrossing, i.e., the amplitude that reappears in the Q space after decaying to the P space. In our earlier paper on four-mode pyrazine we saw a pronounced degree of IC recrossing. We conjectured that this was due to the limited size of the pyrazine model used. Figures 2(b) and 2(c) show $P_2(t)$ (solid lines) and $J(t)^2$ (dashed lines) for the five basis states of Fig. 2(a). It is obvious that $J(t)^2$ follows $P_2(t)$ fairly closely, indicating only a moderate amount of IC recrossing, consistent with expectation.

This behavior seems in stark contrast to that of Fig. 2(d), where $P_2(t)$ and $J(t)^2$ for the $|S_0,0\rangle$ state of Fig. 1 are shown. One might surmise that the rapid falloff of $J(t)^2$ compared to $P_2(t)$ would be an indication of strong IC recrossing, but this is not the case. Rather, the $|S_0,0\rangle$ state is initially a superposition of vibrational states in S_2. Thus, the autocorrelation decay out of the initial $|S_0,0\rangle$ state reflects not just the IC between surfaces but also the nonstationary dynamics of the initial vibrational wave packet on the S_2 surface. The latter source of decay is, in fact, responsible for the fast decay of $J(t)^2$ shown in Fig. 2(d).

B. Resonance structure

The resonance line shape of a basis state $|\kappa\rangle$ is defined as $|\langle\kappa|\gamma\rangle|^2$, i.e., the square of the projection of the exact eigenstates on state $|\kappa\rangle$ as a function of the energy E_γ. This line shape, which is directly connected to observations, often gives a good indication of the dynamics of the system. In our earlier studies of pyrazine,[14] we showed that the system resonance line shapes play a significant role in predicting the coherent controllability of a system. Specifically, we showed that a pair of system states is controllable only if either (a) the resonances of the pair overlap significantly or (b) they both simultaneously overlap a third resonance. In this earlier

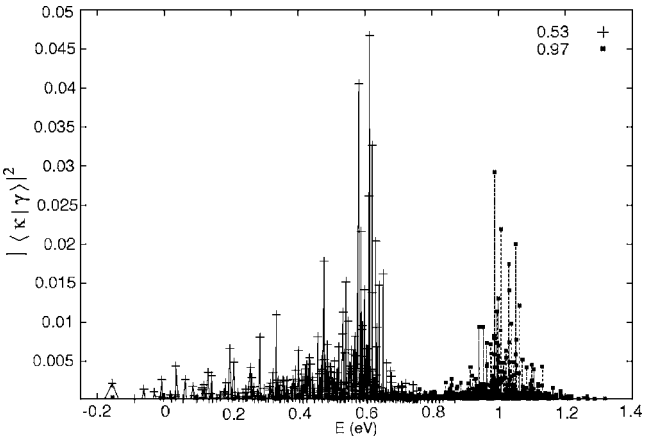

FIG. 3. Resonance line shapes for 0.53 and 0.97 eV states of pyrazine.

work[14] on four-mode pyrazine, we observed diffuse, structureless resonances, displaying a picket-fence-like structure with ill-defined overall shape. This behavior was contrary to what would be expected if the S_2 states decayed into a quasicontinuum of S_1 states—the case, we believed, for pyrazine. This contradictory situation motivated us to examine the resonance structure of pyrazine more closely using the full 24-mode model, as is done here.

Figure 3 shows two typical resonance line shapes obtained in our calculations: the left most resonance is centered on a bare state $|\kappa\rangle$ of energy $\approx$0.53 eV and the resonance on the right is centered at 0.97 eV. Note that this graph reflects a general trend that we observed in the resonance line shapes: the lower energy resonances tend to be more spread out in energy, peaking at smaller energies.

In order to understand these observations we consider coupling a single Q state located at energy E_c to a set of P states. As depicted in Fig. 4(a), we model the coupling strengths to be a Gaussian function centered about $E=0$. A Q state placed at $E_c=0$ yields the symmetric bimodal resonance line shape displayed in Fig. 4(b). As shown in Fig. 4(c), when the resonance center is shifted to small $E_c>0$, the bimodal structure loses its symmetry, displaying a typical Fano-type shape (normally discussed for continuum cases): The peak closer to E_c gets larger and the resonance tails off more into the negative energy domain. As the width of the Gaussian in Fig. 4(a) increases, the center of the right peak of Fig. 4(c) approaches E_c while the left peak vanishes. In the limit of infinite width, Fig. 4(c) transforms into the Lorentzian shape of Fig. 4(d), typical of constant IC coupling.

The above model provides a good explanation of the trend shown in Fig. 3. When we coarse grain the *QHP* IC coupling of the two bare states of Fig. 3 we obtain the curves shown in Fig. 5. Notice how the Hamiltonian for the $E_c=0.53$ eV ket (marked with the left downward arrow) has much more curvature around E_c compared to the coupling for the $E_c=0.97$ eV resonance (marked with the right upward arrow). Thus the resonance at $E_c=0.53$ eV seen in Fig. 3 is analogous to the resonance in Fig. 4(c), with the strong left shift in the resonance due to the strong coupling elements at more negative energies. In contrast, the resonance at $E_c=0.97$ eV is more likely the resonance of Fig. 4(d), with the variation in the coupling much less pronounced, consequently yielding a single peaked Bixon-Jortner shape.

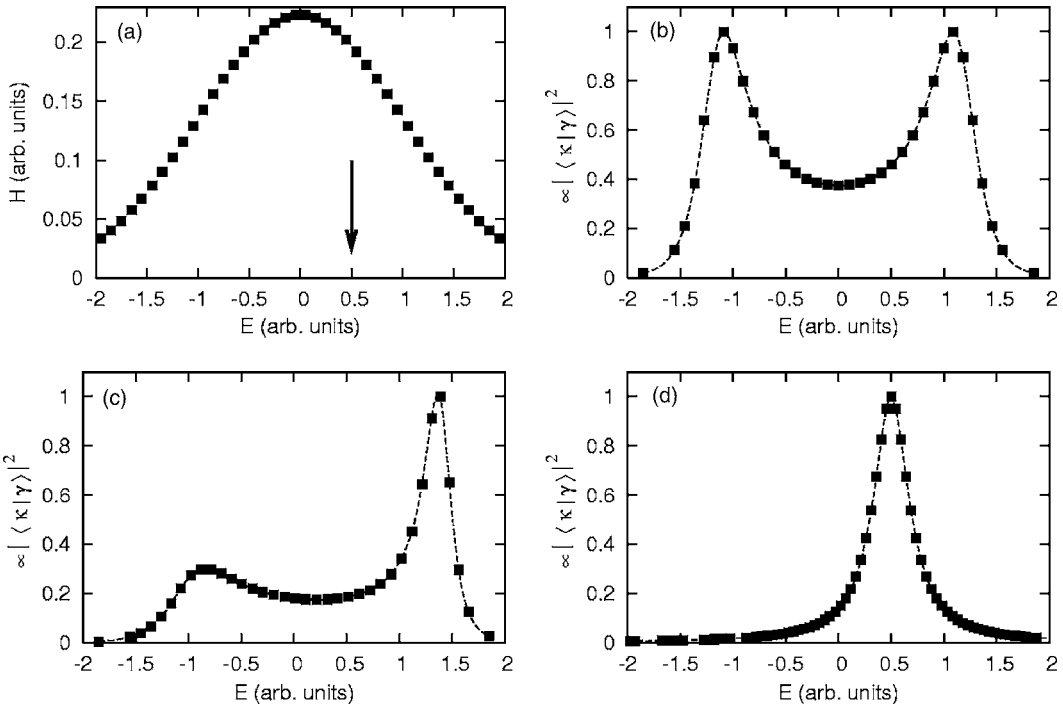

FIG. 4. (a) Model Gaussian-shaped *QHP* IC couplings as a function of the bare state energies. (b) Resonance structure for the *QHP* given by panel (A) when the resonance is centered at $E_c=0$. (c) The same when the resonance is centered at $E_c=0.5$ [arrow of panel (A)]. (d) Resonance characterized by energy independent couplings, centered at $E_c=0.5$. In panels (A), (B), and (C) the *P*-space basis states are located at evenly spaced 0.1 energy intervals. Panel (D) has the *P*-state energies evenly spaced at 0.05, with *QHP* characterized by a constant coupling of 0.055.

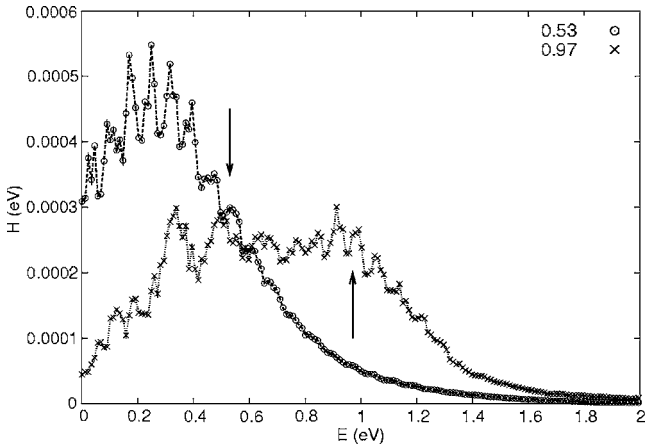

FIG. 5. Coarse-grained IC coupling *PHQ* in pyrazine as a function of energy. Each point has been averaged over ten bins to smooth out very fast fluctuations.

Resonance line shapes provide an energy space perspective that is complementary to the time dependent picture. For example, it can be shown that for $|\langle\kappa|\gamma\rangle|^2 \propto e^{-a(E-E_0)^2}$ Gaussian line shapes, $J(t)^2 = e^{-(t/\tau)^2}$ with $\tau = \sqrt{2\hbar^2 a}$. For Gaussian line shapes the autocorrelation lifetime τ is related to Δ the full width at half maximum (FWHM) of the resonance line shape as $\tau = 1.55$ (eV fs)$/\Delta$. Similar results hold for Lorentzian line shapes. However, when the resonance line shape has bimodal or higher complexity, this inverse relationship no longer holds.

Figure 6 shows resonances for the states at energies of 0.76 and 0.97 eV, whose $J(t)^2$ are shown in Figs. 2(b) and 2(c). The FWHM, estimated from the resonances in Fig. 6, are about 0.02 eV for the 0.76 eV state and about 0.1 eV for the 0.97 eV state. These numbers give τ of approximately 78 and 16 fs, respectively, which are in qualitative agreement with results of Fig. 2. The agreement is less favorable when one looks at the resonance line shapes of Fig. 3. Here, the 0.53 eV resonance has a width of $\approx$0.2 eV, twice as wide as the 0.97 eV resonance. Yet, the $J(t)^2$ functions of Fig. 2(b) are approximately the same. In fact, the τ from Fig. 2 for the 0.53 eV resonance is slightly less than that for the 0.97 eV resonance. Clearly, the decay times derived from Fano-type line shapes are not simply proportional to Δ^{-1}.

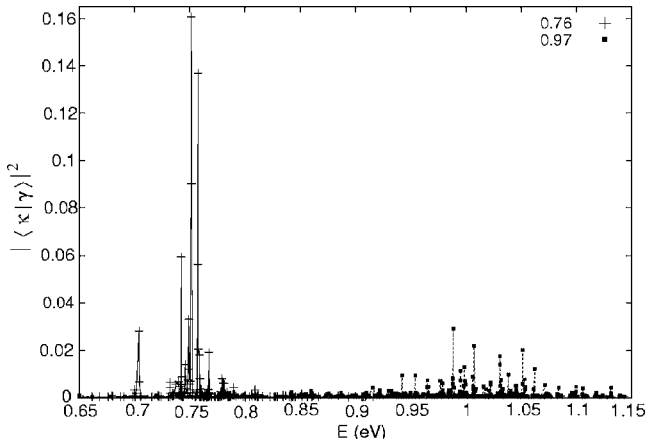

FIG. 6. The resonance line shapes of the 0.76 and 0.97 eV S_2 states in pyrazine.

IV. DISCUSSION

We have presented an efficient method based on partitioning theory to compute bound state dynamics of complex molecular systems for which the P space is readily diagonalizeable. The method has very favorable N_T^2 scaling properties and very modest core requirements even for very large matrices. We have used this method to study the very substantial problem of IC dynamics and resonance line shapes of 24-mode pyrazine. Future work will include the coherent control of IC in 24-mode pyrazine and extending the work of Frishman and Shapiro[28] to the full quantum calculation of spontaneous emission of complex molecules.

Two improvements of the QP algorithm can be considered. As shown above, the QP algorithm scales as N_Q^4. Although N_Q is assumed to be much smaller than N_P, nevertheless its size may represent a non-negligible obstacle. It is possible to incorporate a procedure by which one breaks $\tilde{H}$ up into several smaller matrices and diagonalizes these smaller matrices as needed. A second improvement would result from incorporating matrix deflation into the procedure. This would result in two advantages. First, at present, if one does a calculation which gives unacceptable values for the metric of Eq. (13), one has to repeat the entire calculation with a denser set of grid points. It would be beneficial to use the eigenstates that have already been found in the first calculation in this second calculation. Second, the QP algorithm tends to find eigenstates with larger Q-space overlap more readily than states with small Q-space overlap. That is, the large Q-space vectors tend to mask the smaller Q-space vectors. Both of these issues suggest that it would be useful if one could project out of the original Hamiltonian the subspaces corresponding to eigenstates that have already been found. The well known technique of deflation[29] does just this.

ACKNOWLEDGMENTS

One of the authors (P.S.C.) thanks H.-D. Meyer, L. S. Cederbaum, and G. A. Worth for pyrazine data and for their advice on their pyrazine model. This work was supported by the Natural Sciences and Engineering Research Consul of Canada.

APPENDIX A: DERIVATION OF EQUATION (7)

Here we derive Eq. (7) for the bound state case, following in close analogy to the continuous case of Ref. 13. Starting with the time independent Schrödinger equation and using $Q+P=1$ we have

$$E_\gamma|\gamma\rangle = H|\gamma\rangle = H(P+Q)|\gamma\rangle. \tag{A1}$$

Multiplying this equation on the right by Q or P, and remembering that $Q=Q^2$ and $P=P^2$, gives two equations

$$(E_\gamma - PHP)P|\gamma\rangle = PHQ|\gamma\rangle, \tag{A2}$$

$$(E_\gamma - QHQ)Q|\gamma\rangle = QHP|\gamma\rangle. \tag{A3}$$

Equation (A2) can be inverted to give

$$P|\gamma\rangle = (E_\gamma - PHP)^{-1}PHQ|\gamma\rangle, \tag{A4}$$

where we assume $(E_\gamma - PHP)$ is uniquely invertible. Using Eq. (A4) in the right hand side of Eq. (A3) gives the equation

$$(E_\gamma - QHQ)Q|\gamma\rangle = QHP(E_\gamma - PHP\rangle^{-1}PHQQ|\gamma\rangle. \tag{A5}$$

Rearranging this equation gives Eq. (7) with the $\tilde{H}$ operator given by

$$\tilde{H}(E_\gamma) = QHQ + QHP(E_\gamma - PHP)^{-1}PHQ. \tag{A6}$$

Taking matrix elements of this operator, identifying $QHP = QV_{\mathrm{IC}}P$, and using the spectral resolution

$$(E_\gamma - PHP)^{-1} = \sum_\beta \frac{|\beta\rangle\langle\beta|}{E_\gamma - \epsilon_\beta} \tag{A7}$$

yield Eq. (8).

APPENDIX B: DEGENERACY IN THE QP ALGORITHM

Let there be a Hamiltonian such that there is a set of $M > N_Q$ degenerate eigenstates, $\{|\gamma\rangle\}^M$. We wish to show that one can transform this set of eigenstates (by taking appropriate linear combinations) into two new sets

$$\{|\gamma\rangle\}^M \rightarrow \{|\theta\rangle\}^{N_Q} + \{|\phi\rangle\}^{M-N_Q}, \tag{B1}$$

where all the states $|\theta\rangle$ and $|\phi\rangle$ are orthonormal eigenstates of the Hamiltonian, and all the elements of the second set have the property $Q|\phi\rangle = 0$.

We label $\{|\gamma_1\rangle, \ldots, |\gamma_M\rangle\} \equiv \{|\gamma\rangle\}^M$. Assume that all eigenstates have nonzero Q-space overlap. If this were not the case, then one would reduce the size of the initial set until this was true. Create a set of vectors, $\{|z_i\rangle\}$, all of which, except one, are orthogonal to a vector $|\kappa\rangle$ in the Q space. Then we have (assuming that $\langle\kappa|\gamma_1\rangle \neq 0$ which must be true for at least one γ)

$$\begin{aligned} |z_1\rangle &= |\gamma_1\rangle, \\ |z_2\rangle &= C_2[|\gamma_2\rangle - \alpha_{21}|\gamma_1\rangle], \\ &\vdots \\ |z_M\rangle &= C_M[|\gamma_M\rangle - \alpha_{M1}|\gamma_1\rangle], \end{aligned} \tag{B2}$$

where C_i normalizes the states and

$$\alpha_{ij} = \frac{\langle\kappa|\gamma_i\rangle}{\langle\kappa|\gamma_j\rangle}. \tag{B3}$$

Clearly $\langle\kappa|z_i\rangle = 0$ unless $i=1$. Next, form a new set of vectors, $\{|y_i\rangle\}$, that are orthonormalized via Gram-Schmidt orthogonalization

$$\begin{aligned} |y_M\rangle &= |z_M\rangle, \\ |y_{M-1}\rangle &= D_{M-1}[|z_{M-1}\rangle - |y_M\rangle\langle y_M|z_{M-1}\rangle], \\ &\vdots \\ |y_n\rangle &= D_n\left[|z_n\rangle - \sum_{k=n+1}^{M} |y_k\rangle\langle y_k|z_n\rangle\right], \\ &\vdots \\ |y_1\rangle &= D_1\left[|z_1\rangle - \sum_{k=2}^{M} |y_k\rangle\langle y_k|z_1\rangle\right]. \end{aligned} \tag{B4}$$

Notice that $\langle\kappa|y_i\rangle = 0$ unless $i=1$, and if $i=1$ then $\langle\kappa|y_1\rangle \propto \langle\kappa|\gamma_1\rangle \neq 0$. We define $|\theta_1\rangle \equiv |y_1\rangle$, and we are left with the set $\{|\theta_1\rangle, |y_2\rangle, \ldots, |y_M\rangle\}$. An advantage of this set is that one can take any linear combination of $\{|y_2\rangle, \ldots, |y_M\rangle\}$ and that vector is also orthogonal to $|\kappa\rangle$. This begs one to repeat the above algorithm using the set $\{|y_2\rangle, \ldots, |y_M\rangle\}$ and considering a different member of the Q space, $|\kappa'\rangle$. This would result in a new set of vectors $\{|\theta_1\rangle, |\theta_2\rangle, |y_3\rangle, \ldots, |y_M\rangle\}$, such that $\{|y_3\rangle, \ldots, |y_M\rangle\}$ were orthogonal to both $|\kappa\rangle$ and $|\kappa'\rangle$. Naturally, this process can be repeated until all the Q-space bare states had been used, resulting in a set $\{|\theta_1\rangle, \ldots, |\theta_{N_Q}\rangle, |y_{N_Q+1}\rangle, \ldots, |y_M\rangle\}$. This last set has exactly the properties of Eq. (B1), where $\{|y_{N_Q+1}\rangle, \ldots, |y_M\rangle\}$ are all orthogonal to the whole of the Q space.

APPENDIX C: NORMALIZATION OF $|D_\gamma\rangle$

Recall that any constant multiple of an eigenstate is also an eigenstate. Typically, when an eigensolver completes the diagonalization, it assures that all the eigenstates are normalized to unity. This means that our calculation ends up with a state $|D_\gamma\rangle$ such that

$$\langle D_\gamma|D_\gamma\rangle = 1, \tag{C1}$$

$$C_\gamma|D_\gamma\rangle = Q|\gamma\rangle, \tag{C2}$$

for some constant C_γ. That is, the solution we obtain from the QP algorithm is proportional to $Q|\gamma\rangle$. We must still compute the constant of proportionality, which is the subject of this appendix. Remembering that $1 = Q + P$, $Q = Q^2$, and $P = P^2$, we write

$$\langle\gamma|\gamma\rangle = \langle\gamma|Q|\gamma\rangle + \langle\gamma|P|\gamma\rangle = \langle\gamma|Q^2|\gamma\rangle + \langle\gamma|P^2|\gamma\rangle, \tag{C3}$$

$$\langle\gamma|Q^2|\gamma\rangle = |C_\gamma|^2\langle D_\gamma|D_\gamma\rangle = |C_\gamma|^2, \tag{C4}$$

$$\langle\gamma|P^2|\gamma\rangle = \langle\gamma|QHP[E_\gamma - PHP]^{-1}[E_\gamma - PHP]^{-1}PHQ|\gamma\rangle, \tag{C5}$$

where the last equality uses Eq. (A4). Then using the spectral resolution, Eq. (A7) and (C5) becomes

$$\langle\gamma|P^2|\gamma\rangle = \sum_{\beta} \frac{\langle\gamma|QH|\beta\rangle\langle\beta|HQ|\gamma\rangle}{(E_\gamma - \epsilon_\beta)^2}, \tag{C6}$$

which using Eq. (C2) gives

$$\langle\gamma|P^2|\gamma\rangle = |C_\gamma|^2 \sum_{\beta} \frac{\langle D_\gamma|H|\beta\rangle\langle\beta|H|D_\gamma\rangle}{(E_\gamma - \epsilon_\beta)^2}. \tag{C7}$$

Then with Eqs. (C7) and (C3) we can write

$$1 = |C_\gamma|^2 \left(1 + \sum_{\beta} \frac{\langle D_\gamma|H|\beta\rangle\langle\beta|H|D_\gamma\rangle}{(E_\gamma - \epsilon_\beta)^2}\right), \tag{C8}$$

which allows one to compute the normalization factor C_γ. Note that it is only the magnitude of C_γ that is relevant, the phase is irrelevant. This can be seen as follows. C_γ sets the phase for $Q|\gamma\rangle$, which in turn sets the phase for $|\gamma\rangle$. Consider the propagator in terms of the eigenstates

$$U(t) = \sum_{\gamma} e^{-iE_\gamma t}|\gamma\rangle\langle\gamma|. \tag{C9}$$

It can readily be seen that any eigenstate $|\gamma'\rangle$ can be replaced by $e^{i\theta}|\gamma'\rangle$ for any real θ without changing the propagator of the above equation. Thus the phase of $|\gamma\rangle$ is irrelevant, and by reversing the above logic, the phase of C_γ is irrelevant.

[1] U. Fano, Nuovo Cimento **12**, 156 (1935).
[2] U. Fano, Phys. Rev. **124**, 1866 (1961).
[3] H. Feshbach, Ann. Phys. (N.Y.) **5**, 357 (1958).
[4] P. O. Löwdin, J. Math. Phys. **3**, 969 (1962).
[5] P. O. Löwdin, J. Mol. Spectrosc. **10**, 12 (1963).
[6] M. Shapiro, J. Chem. Phys. **56**, 2582 (1972).
[7] M. Shapiro, J. Phys. Chem. **102**, 9570 (1998).
[8] A. Raab, G. A. Worth, H.-D. Meyer and L. S. Cederbaum, J. Chem. Phys. **110**, 936 (1999).
[9] V. Stert, P. Farmanara, and W. Radloff, J. Chem. Phys. **112**, 4460 (2000).
[10] M. Seel and W. Domcke, J. Chem. Phys. **95**, 7806 (1991).
[11] G. Stock and W. Domcke, J. Chem. Phys. **97**, 12466 (1993).
[12] A. L. Sobolweski, C. Woywod, and W. Domcke, J. Chem. Phys. **98**, 5627 (1993).
[13] M. Shapiro and P. Brumer, *Principles of the Quantum Control of Molecular Processes* (Wiley, New Jersey, 2003).
[14] P. S. Christopher, M. Shapiro, and P. Brumer, J. Chem. Phys. **123**, 064313 (2005).
[15] P. S. Christopher, M. Shapiro, and P. Brumer (in preparation).
[16] A. R. Gourlay and G. A. Watson, *Computational Methods for Matrix Eigenproblems* (Wiley, London, 1973).
[17] Y. Saad, *Numerical Methods for Large Eigenvalue Problems* (Manchester University Press, Manchester, UK, 1992).
[18] We quote here the scaling of the Householder tridiagonalization followed by the QR algorithm, which is regarded as the best general purpose diagonalization method (Refs. 16 and 17). There are several methods to compute extreme eigenvectors/eigenvalues (e.g., Lanczos method), but because we are interested in the dynamics of our system, we require all (or most) of the eigenvectors/eigenvalues.
[19] A. A. Sanz, P. S. Christopher, M. Shapiro, and P. Brumer (in preparation).
[20] Eigensolvers tend to order the eigenvalues in increasing order, so we know what order the eigenvalues are in. But that does not help us preserve the order of the eigenvalues from one grid point to the next.
[21] The grid points are put down so that their density is proportional to the bare state density of states.
[22] Note, however, that the coarse graining method described in the next section allows one to get very good QP-algorithm performance even if $N_Q \approx N_P$.
[23] The technique of using a window of nearby states seems to work well, based on the fact that the denominator of the second term of Eq. (14) makes nearby states the important part of the expansion.
[24] Also note that this definition for $|\alpha\rangle$ means that $\mathrm{Tr}(|\alpha\rangle\langle\alpha|)=1$. That is, $\mathrm{Tr}(|\alpha\rangle\langle\alpha|)=\Sigma_\gamma\langle\gamma|\alpha\rangle\langle\alpha|\gamma\rangle=1/\varrho_\alpha\Delta_\alpha(\Sigma_{\gamma\in A_\alpha}1)=1$.
[25] R. Borrelli and A. Peluso, J. Chem. Phys. **119**, 8437 (2003).
[26] M. Thoss, W. H. Miller, and G. Stock, J. Chem. Phys. **112**, 10282 (2000).
[27] A less detailed calculation was also presented by Raab *et al.* in the same paper. This calculation took only 100 CPU hours and was designed to check the convergence of their calculations. We assume that the larger calculation is the more accurate and thus compare our computations to these results.
[28] E. Frishman and M. Shapiro, Phys. Rev. Lett. **87**, 253001 (2001).
[29] B. N. Parlett, *The Symmetric Eigenvalue Problem* (Prentice-Hall, Englewood Cliffs, NJ, 1980).